Earth and Planetary Science Letters 319-320 (2012) 146–158

Contents lists available at SciVerse ScienceDirect

Earth and Planetary Science Letters

journal homepage: www.elsevier.com/locate/epsl

The age and rate of displacement along the Main Central Thrust in the western Bhutan Himalaya

Tobgay Tobgay [a,*], Nadine McQuarrie [a,1], Sean Long [a,2], Matthew J. Kohn [b], Stacey L. Corrie [b]

[a] Department of Geosciences, Princeton University, Princeton, NJ, 08544, United States
[b] Department of Geosciences, Boise State University, Boise, ID, 83725, United States

ARTICLE INFO

Article history:
Received 24 June 2011
Received in revised form 30 November 2011
Accepted 1 December 2011
Available online xxxx

Editor: T.M. Harrison

Keywords:
Bhutan Himalaya
geochronology
monazite
metamorphism
melting
Main Central Thrust

ABSTRACT

In western Bhutan, the Main Central Thrust (MCT) is broadly folded, creating multiple exposures of the fault surface over a ~70 km across-strike distance. This unusual map pattern presents a unique opportunity to map the MCT and document both the magnitude and age of displacement. In situ Th-Pb (SIMS and LA-ICP-MS) geochronology of metamorphic monazite from the immediate hanging wall of the MCT indicates that prograde monazite growth in Greater Himalayan (GH) rocks continued until 20.8 ± 1.1 Ma, whereas crystallization of in situ melts, characterized by high Y monazite overgrowths, occurred during cooling from ca. 15–10 Ma. Prograde monazite growth at 15 Ma in Lesser Himalaya (LH) rocks in the immediate footwall requires that LH footwall strata began to be buried at this time, and the MCT had reached its southernmost, exposed extent. By combining prograde monazite ages in the immediate hanging wall and footwall, the duration of MCT displacement is bracketed between 20.8 ± 1.1 and 15.0 ± 2.4 Ma. Immediately north of our study area, a published estimate of shearing along the outer-South Tibetan detachment (STD) argues for displacement between 20 and 15 Ma, coeval with the age range for MCT displacement that we document in this study. However retrograde monazite grains as young as 10 Ma suggest that GH rocks were cooling until ~10 Ma, 5 Myr later than motion on the outer-STD immediately to the north. This cooling was either the result of continued displacement on the MCT, or growth of a duplex that passively folded the MCT. Using a sequential reconstruction, we estimate a total displacement of ~230 km, which is the sum of displacements on the MCT and the structurally-lower Paro Thrust, over a duration of 5.8 ± 2.6 Myr. This indicates a horizontal shortening rate of 4.0 + 3.2/− 1.3 cm/yr, which exceeds present rates estimated from geodetic measurements across the Himalaya, and MCT displacement rates (c. 2 cm/yr) inferred from petrologic and thermal models in central Nepal but is indistinguishable from plate convergence rates calculated for eastern Bhutan between 23 and 20 Ma (3.3 ± 0.7 cm/yr). Our study highlights that displacement on the MCT alone achieved plate velocity rates in western Bhutan, and that the age and rate of MCT displacement varied significantly across the Himalaya.

1. Introduction

The Himalayan fold–thrust belt formed in response to ongoing continental convergence between India and Asia that began at ca. 50 Ma (e.g. Hodges, 2000). Today, shortening in the Himalaya is estimated to take up nearly one-third of the 5.8 ± 0.4 cm/yr India–Asia convergence rate (e.g. Bilham et al., 1997; Larson et al., 1999). Spanning the entire length of the orogen, the Main Central Thrust [MCT; or thrust contact between Greater and Lesser Himalayan (GH and LH) rocks] has accommodated a large percentage of the total shortening in the Himalaya (e.g. Hodges, 2000; Yin and Harrison, 2000) (Fig. 1).

Numerous studies have focused on the timing of MCT displacement, which strongly influences views of orogenic evolution. For example, were displacement rates and timing constant (within error) across strike, or did they vary? If they varied, did they do so systematically or chaotically, and how was overall convergence otherwise partitioned? Taken together, the broad sweep of monazite ages in the Himalaya indicates earliest MCT movement in the early Miocene (e.g. Catlos et al., 2001; 2004; Chambers et al., 2011; Harrison et al., 1998; Hodges et al., 1996; Kohn et al., 2004), but inconsistent levels of detail hide potential variations in displacement rates along the MCT. To differentiate rates and their tectonic drivers more targeted comparisons are required. For example, data from central Nepal indicate ca. 5 Ma differences in timing for MCT movement (Corrie and Kohn, 2011; Kohn, 2008) and possible large variations in displacement rates (Kohn et al., 2004). Comparable studies elsewhere in the Himalaya are as yet lacking, prohibiting orogenic generalization.

* Corresponding author.
E-mail address: ttobgay@princeton.edu (T. Tobgay).
[1] Now at University of Pittsburgh, Pittsburgh, PA 15260, United States.
[2] Now at University of Nevada, Reno, NV 89557, United States.

0012-821X/$ – see front matter © 2011 Elsevier B.V. All rights reserved.
doi:10.1016/j.epsl.2011.12.005

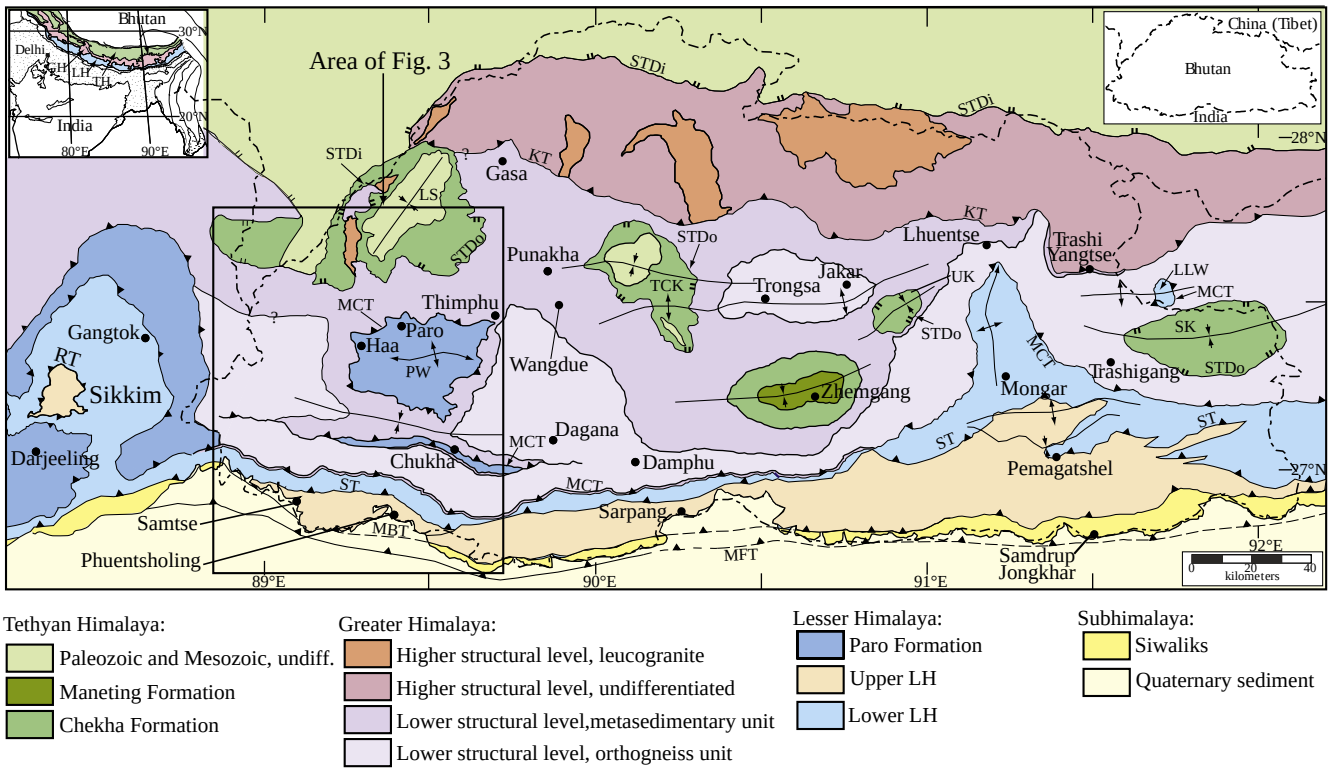

Fig. 1. Simplified geologic map of Bhutan and surrounding region modified from Long et al. (2011c). Upper-left inset shows generalized geologic map of the Himalayan orogen (modified from Gansser, 1983). Upper-right inset shows the international boundary of Bhutan. Our study area (Fig. 3) is shown by a rectangular box. Abbreviations: TH — Tethyan Himalaya; GH — Greater Himalaya; LH — Lesser Himalaya; STDo — outer-South Tibetan detachment; STDi — inner-South Tibetan detachment; KT — Kakhtang Thrust; MCT — Main Central Thrust; MBT — Main Boundary Thrust; MFT — Main Frontal Thrust; ST — Shumar Thrust; RT — Ramgarh Thrust; PW — Paro window; LS — Lingshi syncline; TCK — Tang Chu klippe; UK — Ura klippe; SK — Sakteng klippe; LLW — Lum La window (location from Yin et al., 2010). Map of Sikkim region modified from McQuarrie et al. (2008). Baxa Formation in the footwall of RT in Sikkim from Bhattacharyya and Mitra (2009). Map projection — geographic lat/long (WGS84).

Few data are available in Bhutan to constrain the timing of MCT movement. In eastern Bhutan MCT movement is thought to have occurred between 22 and 16 Ma, based on bulk monazite ages from GH gneisses and LH schist collected immediately adjacent to their mutual contact (Daniel et al., 2003). In western Bhutan, no information exists on the actual age of MCT displacement. However, multiple exposures of the MCT and varying structural levels of the GH section in its hanging wall allowed us to sample over a ~70 km across-strike distance. Few other locations in the Himalaya expose such large across-strike distances for any major shear zone, and none has yet been explored chronologically for the unique tectonic information available from such exposures. In principle, across-strike exposures allow resolution of timing and rates of shear zone movement independent of thermal–mechanical models that other studies have relied upon (e.g., Corrie and Kohn, 2011; Kohn, 2008; Kohn et al., 2004).

Here, we present chemically-defined Th–Pb in situ monazite ages from GH rocks immediately above the MCT in western Bhutan in combination with a balanced geologic cross-section to define a minimum amount of displacement. These data allow us to specifically evaluate both the timing and rates of displacement on the MCT. By combining our data with published monazite data further north in Bhutan (Kellett et al., 2010), we compare the age of MCT displacement to proposed coeval deformation of the GH section and displacement on the South Tibetan detachment (STD). We also assess along-strike variations in initiation of MCT motion in comparison with data ~150 km to the east (Daniel et al., 2003).

2. Geologic background and samples

The western Bhutan Himalaya was chosen for this study because; i) GH rocks in western Bhutan have experienced high deformation temperatures. GH rocks exhibiting partial melt textures (leucocratic segregation surrounded by melanosome; Fig. 2) extend southward to within 15 km of the deformation front. The presence of deformed kyanite together with partial melt distributed through most of the section (Fig. 2) constrains a minimum temperature of >700 °C (Spear et al., 1999). Chemical reactions associated with partial melting are important for understanding chemical systematics of monazite (Kohn et al., 2005; Spear and Pyle, 2002; Spear et al., 1999). ii) Folding of the MCT and overlying GH thrust sheet has resulted in multiple exposures over an across-strike distance of ~70 km, which provides a unique opportunity to map and sample the MCT and GH section in multiple locations.

The first-order tectonostratigraphic subdivisions and major bounding faults from south to north in western Bhutan are the Main Frontal Thrust (MFT), the Subhimalayan zone (a.k.a. Siwalik Group), Main Boundary Thrust (MBT), Lesser Himalayan (LH) zone, Main Central Thrust (MCT), Greater Himalayan (GH) zone, South Tibetan detachment (STD), and the Tethyan Himalayan (TH) zone (e.g. Gansser, 1964, 1983; Hodges, 2000; Le Fort, 1975; Yin, 2006) (Fig. 3). The Siwalik Group consists of Miocene to Pliocene synorogenic deposits that are bound at their base by the MFT (e.g. DeCelles et al., 2004; Gansser, 1964, 1983; Tukuoka et al., 1986).

The LH zone consists of clastic and carbonate metasedimentary rocks and is divided into two stratigraphic successions: the Paleoproterozoic lower Lesser Himalayan section, and the Neoproterozoic–Paleozoic upper Lesser Himalayan section (Long et al., 2011a; McQuarrie et al., 2008). The lower Lesser Himalayan section consists of the Shumar Formation (containing fine-grained and medium- to thick-bedded, cliff-forming quartzite with schist and phyllite interbeds) and Daling Formation (schist and green phyllite with quartzite interbeds), which are collectively referred to as the Daling–Shumar

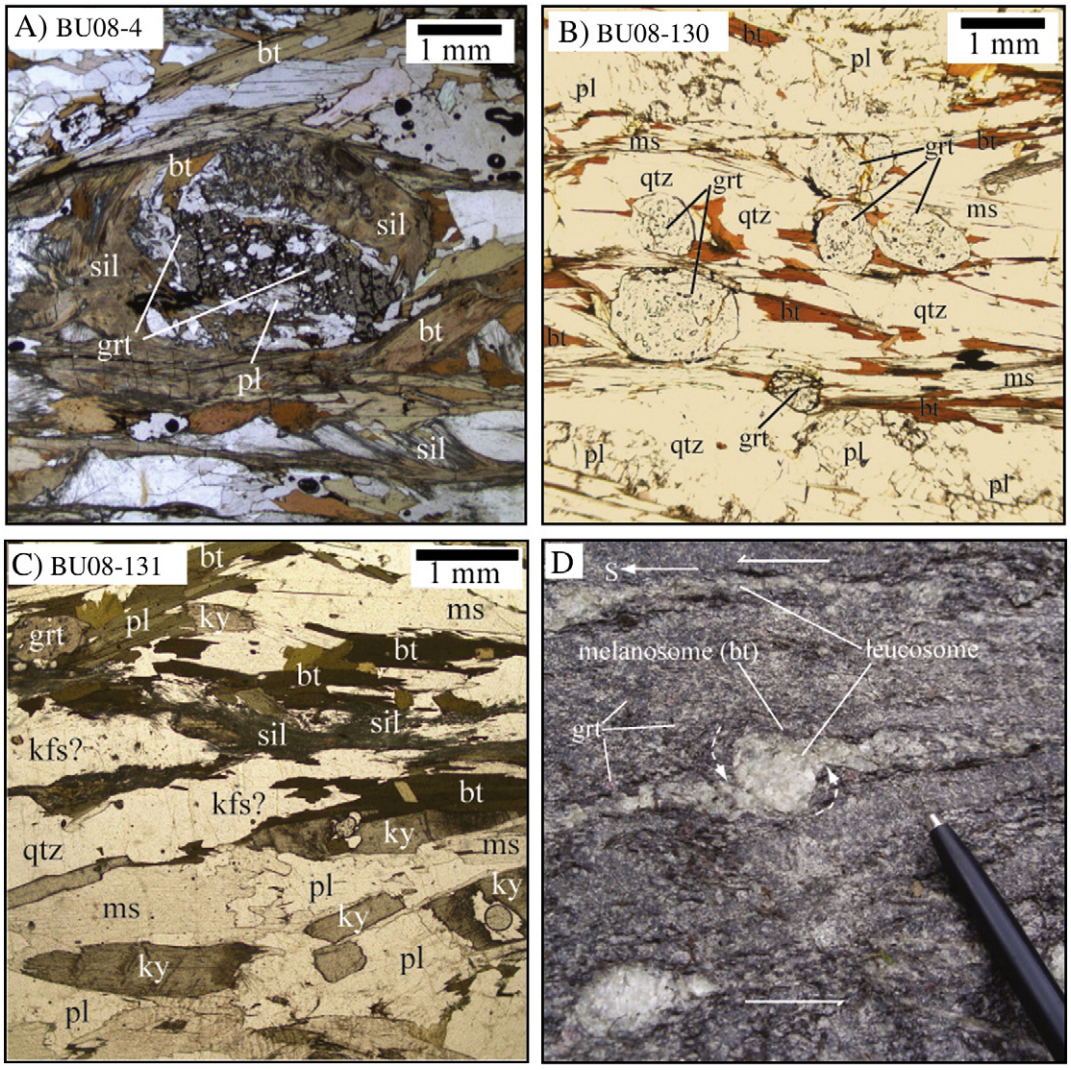

Fig. 2. A)–D) Photomicrographs of GH rocks taken in plane polarized light showing breakdown of garnet (rounded or replaced grains), which is the likely source of Yttrium (Y) in monazite, to form sillimanite and biotite. In these rocks, the likely retrograde reaction is grt + kfs + melt = bt + sil (melting reaction 12 of Spear et al. (1999) in retrograde sense). Refer to Fig. 3 for sample locations and Table S1 for mineral assemblages. A) Sample BU08-4, with assemblage qtz + bt + grt + pl + sil + kfs. B) Sample BU08-130, with assemblage qtz + bt + grt + pl + ky + sil + kfs + st. C) Sample BU08-131, with deformed kyanite in presence of qtz + bt + grt + pl + sil + kfs. D) Photograph showing leucocratic segregation (leucosome + biotite = gneiss) (Longitude: 89.25575°E, Latitude: 27.24893°N). Mineral abbreviations: qtz — quartz, ms — muscovite, bt — biotite, grt — garnet, st — staurolite, ky — kyanite, sil — sillimanite, kfs — K-feldspar, pl — plagioclase.

Group. The Neoproterozic–Paleozoic upper Lesser Himalayan section consists of three units, the Baxa Group, Jaishidanda Formation, and Paro Formation. The Baxa Group consists of dark gray to black slate and phyllite, creamy dolomite, white to pink marble and fine to medium grained quartzite. The Baxa Group is separated from the underlying Siwaik Group by the MBT (Fig. 3). The Jaishidanda Formation is a thin (~0.5–1 km) interval of light-gray, biotite-rich quartzite, interbedded with biotite–garnet schist that is exposed immediately below the MCT (Fig. 3). The Paro Formation consists of quartzite, quartzite–garnet–schist, marble, and minor calc-silicate rocks. It is intruded by two mica–garnet orthogneiss and is interpreted as the northern (distal) equivalent of the Jaishidanda Formation (Tobgay et al., 2010).

The GH zone in western Bhutan consists of lower metasedimentary and orthogneiss units, and an upper metasedimentary unit exposed only in the northern and eastern portions of the map area (e.g. Long et al., 2011d) (Fig. 3). The lower metasedimentary unit is Neoproterozoic–Cambrian in age and consists of paragneiss containing staurolite, kyanite, and sillimanite, muscovite–biotite–garnet schist, and quartzite. In western Bhutan it is ~5.0–6.0 km thick and dominates GH rock exposure (Long et al., 2011d). This lower metasedimentary unit is separated from the underlying Jaishidanda Formation in the south and Paro Formation in the north by the MCT (Fig. 3). The orthogneiss unit is granitic in composition and represents a deformed Cambro–Ordovician granite pluton that intruded GH sedimentary protoliths (Long and McQuarrie, 2010).

The TH zone is separated from the underlying GH zone by the outer-STD. The outer-STD is a ductile shear zone with top-to-the-north shear sense that is located closer to the orogenic front (farther south) than the inner-STD along the high Himalayan peaks (e.g. Grujic et al., 2002; Fig. 1). The TH zone consists of Neoproterozoic to Mesozoic sedimentary rocks that were deposited on the distal part of the northern Indian margin (e.g. Garzanti, 1999).

The tectonostratigraphy described above is overprinted by a progressive increase in metamorphic grade, from garnet–biotite–muscovite in the LH Jaishidanda Formation beneath the MCT in the south, to staurolite–muscovite, kyanite–muscovite, sillimanite–muscovite, and finally sillimanite–K-feldspar (muscovite out) in GH rocks above the MCT in the north. This apparent inversion of metamorphic grade occurs within an across-strike distance of <15 km from the southern trace of the MCT. The MCT is commonly mapped as the boundary between GH and LH rocks based on both a lithologic and metamorphic

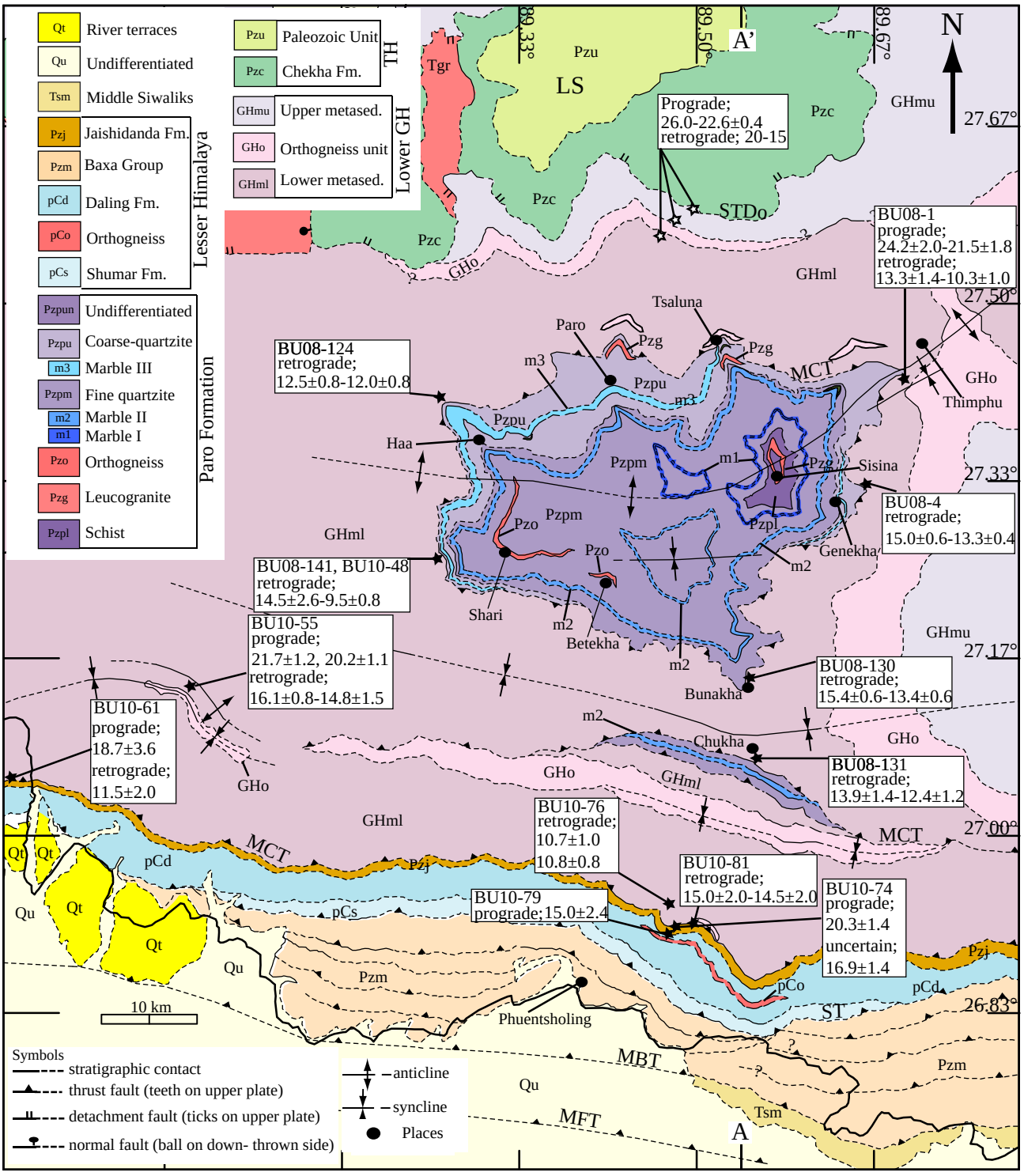

Fig. 3. Geologic map of western Bhutan (modified from Long et al., 2011d) (see Fig. 1 for location and structure abbreviations). Solid stars are our samples with Th–Pb ages of monazite enclosed in white boxes. Open stars are samples from Kellett et al. (2010) in the north. Note that the GH section is divided into three mappable units (GHmu — upper metasedimentary unit, GHo — orthogneiss unit, and GHml — lower metasedimentary unit) that are not separated by faults. A–A′: cross section line of Fig. 6E. See Fig. 2 for mineral abbreviations. Map projection — geographic lat/long (WGS84).

contrast, although penetrative top-to-the-south shear may extend structurally beneath the MCT into the LH section. In the field, we mapped the southernmost trace of the MCT as a boundary that separates ortho- and paragneiss exhibiting partial melt textures from the underlying LH Jaishidanda Formation, which contains biotite-rich, garnet-bearing schist interbedded with quartzite. Further to the north, the MCT is mapped as a boundary that separates GH rocks from the underlying Paro Formation (Fig. 3), and again this contact coincides with a sharp lithologic and metamorphic change. Immediately above the MCT, GH rocks consist of partially melted kyanite-bearing paragneiss. Here, the additional presence of sillimanite with K-feldspar and leucosome indicates the muscovite dehydration–melting reaction (ms + pl + qtz = sil + kfs + melt) and suggests that these rocks have attained a minimum temperature of 700 °C at a pressure of

8 kbar (e.g. Daniel et al., 2003; Spear et al., 1999). Rocks of the Paro Formation immediately below the MCT are predominantly quartzite with schist interbeds (Tobgay et al., 2010). In addition to accessory minerals, rocks contain quartz, muscovite, biotite, garnet, and rare staurolite with kyanite only in the lowest part of the section. Together with quartz recrystallization microstructures that indicate deformation temperatures of ~500–630 °C, these assemblages suggest distinctly lower metamorphic grades in the footwall of the MCT (Tobgay et al., 2010).

Samples were collected from the GH section, with one additional sample from the Jaishidanda Formation just beneath the MCT, along two N–S transects in western Bhutan. Sampling transects extended between the immediate footwall of the southernmost trace of the MCT to north of the GHS–Paro Formation contact (Fig. 3). GH samples for Th–Pb geochronology include paragneiss and schist collected within ~650 m structural distance above the MCT, and a LH schist sample collected from ~50 m below the MCT (Fig. 3; Table S1).

3. Monazite chemistry

We focused on monazite, a LREE–phosphate, because it incorporates significant amounts of U (up to 1 wt.%) and Th (up to 10 wt.%) (Spear and Pyle, 2002), contains little or no common Pb (<1 ppm; Parrish, 1990), and is resistant to radiogenic Pb-loss via diffusion during metamorphism (Catlos et al., 2002; Cherniak et al., 2004; Harrison et al., 2002; Parrish, 1990; Smith and Giletti, 1997). As has been discussed extensively, monazite growth and chemistry in metapelitic rocks are directly linked to reactions involving silicate minerals, particularly garnet (Corrie and Kohn, 2008; Kohn and Malloy, 2004; Pyle and Spear, 2003; Pyle et al., 2001; Spear and Pyle, 2002; Wing et al., 2003). Key to interpreting monazite ages is the recognition of Yttrium (Y) and Thorium (Th) as chemical tracers that are strongly and systematically zoned in response to metamorphic reactions (Kohn and Malloy, 2004; Kohn et al., 2004, 2005; Pyle and Spear, 1999, 2003; Spear and Pyle, 2002).

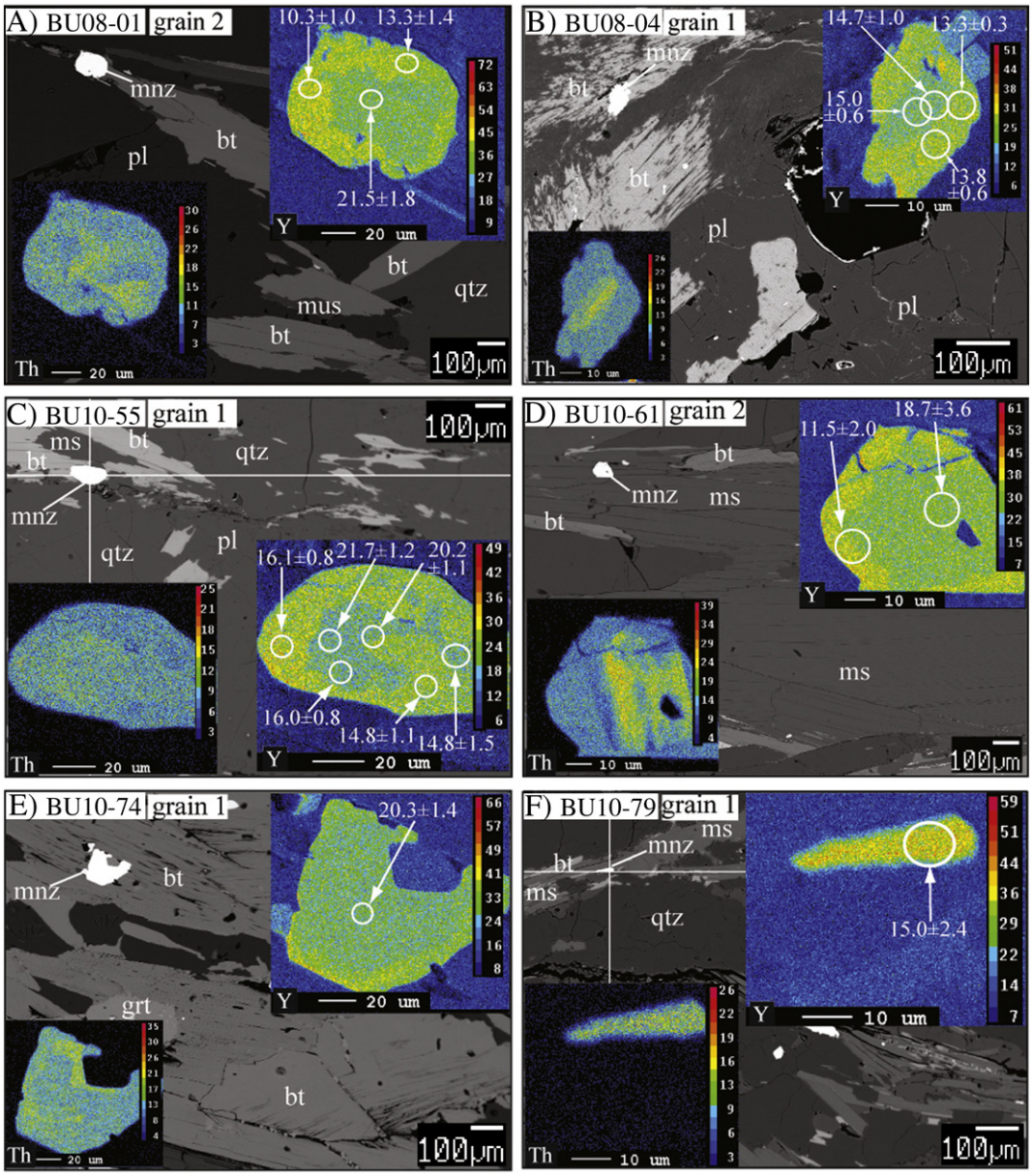

Fig. 4. A)–F) Elemental maps of Y and Th in monazite, illustrating distinct chemical domains. Representative spot analyses are inset in back-scattered electron images that show textural context of in situ monazite (abbreviated mnz). White circles are chronologic analysis spots with ages (listed with 2σ uncertainties). High vs. low concentrations of Y and Th in monazite are denoted by "hot" vs. "cold" colors. Refer Fig. 2 for mineral abbreviations, Fig. 3 for sample locations, and Figs. S1 and S2 for supplementary data. (For interpretation of the references to color in this figure legend, the reader is referred to the web version of this article.)

In principle, Th and Y systematics in monazite can depend on numerous minerals, including garnet, xenotime, and allanite. Allanite has been observed in some LH rocks and may be an important precursor to monazite (e.g. Catlos et al., 2002). Theoretical analysis (Spear, 2010) demonstrates that during prograde metamorphism, allanite breaks down abruptly to form monazite, and this may explain how prograde monazite formed in the LH Jaishidanda Formation. In contrast, we observed no allanite or xenotime in GH rocks, either as matrix grains or inclusions, nor did we find chemical evidence for their former stability (e.g. high-Y garnet cores: Pyle and Spear, 1999, 2003; Spear and Pyle, 2002). Allanite is rarely identified in GH metapelites (allanite as inclusions within garnet was identified by Chambers et al., 2011). Xenotime is more common and was reported within the matrix of GH samples below the STD in western Bhutan (Kellett et al., 2010), as well as in

Table 1
Th–Pb monazite geochronology results.

Analysis	Spot	$^{208}Pb/^{232}Th$				% Radiogenic			
		Age (Ma)	2σ	$^{208}Pb/^{232}Th$	2σ	ThO_2/Th	^{208}Pb	Th/U	Remarks
BU08_1 (grain 1)	3	24.2	2.0	0.00120	0.00010	2.57	95.9	10.9	EP
BU08_1 (grain 1)	2	23.9	2.0	0.00118	0.00010	2.56	95.9	10.7	EP
BU08_1 (grain 1)	4	23.0	2.0	0.00114	0.00010	2.43	96.1	12.2	EP
BU08_1 (grain 1)	5	23.0	2.0	0.00114	0.00010	2.59	96.1	11.3	EP
BU08_1 (grain 1)	1	21.9	1.8	0.00109	0.00008	2.67	95.8	10.8	EP
BU08_1 (grain 2)	1	21.5	1.8	0.00106	0.00010	2.51	95.3	12.2	EP
BU08_1 (grain 2)	3	13.3	1.4	0.00066	0.00006	2.27	87.9	13.9	LR
BU08_1 (grain 2)	2	10.3	1.0	0.00051	0.00004	2.43	91.9	16.4	LR
BU08_4 (grain 1)	1	14.7	1.0	0.00073	0.00004	2.54	88.6	12.1	LR
BU08_4 (grain 1)	1[a]	15.0	0.6	0.00074	0.00003			7.6	LR
BU08_4 (grain 1)	2[a]	13.3	0.4	0.00066	0.00002			6.5	LR
BU08_124 (grain 1)	1	12.0	0.8	0.00059	0.00004	2.37	83.4	7.9	LR
BU08_124 (grain 2)	2	12.3	0.8	0.00061	0.00004	2.53	87.6	9.3	LR
BU08_124 (grain 2)	1	12.5	0.8	0.00062	0.00004	2.66	80.9	7.6	LR
BU08_130 (grain 1)	1	14.0	0.6	0.00069	0.00002	2.56	89.8	9.7	LR
BU08_130 (grain 2)	2	15.4	0.6	0.00076	0.00004	2.23	93.2	10.7	LR
BU08_130 (grain 2)	1	13.4	0.6	0.00066	0.00002	2.38	90.4	10.8	LR
BU08_131 (grain 1)	2	12.4	1.2	0.00061	0.00006	2.33	94.0	15.6	LR
BU08_131 (grain 1)	1	12.6	1.2	0.00062	0.00006	2.43	93.2	14.6	LR
BU08_131 (grain 1)	3	13.9	1.4	0.00069	0.00008	2.35	77.8	15.2	LR
BU08_141 (grain 1)	1	10.5	0.4	0.00052	0.00002	2.07	97.2	8.2	LR
BU08_141 (grain 1)	2	9.5	0.8	0.00047	0.00004	1.81	84.8	9.0	LR
BU10_48 (grain 3)	3	14.0	2.4	0.00069	0.00012	2.75	93.3	9.7	LR
BU10_48 (grain 3)	4	14.5	2.6	0.00071	0.00012	2.72	93.7	8.9	LR
BU10_48 (grain 1)	1	13.5	2.4	0.00067	0.00014	2.47	61.2	10.1	LR
BU10_48 (grain 1)	2	13.2	2.4	0.00065	0.00012	2.64	89.5	8.4	LR
BU10_48 (grain 3)	1	13.0	2.4	0.00065	0.00012	2.56	90.7	7.5	LR
BU10_48 (grain 4)	1	13.0	2.4	0.00064	0.00012	2.62	93.7	10.9	LR
BU10_48 (grain 2)	1	12.6	2.4	0.00062	0.00012	2.61	91.7	10.4	LR
BU10_48 (grain 3)	2	12.3	2.2	0.00061	0.00012	2.63	91.8	7.3	LR
BU10-48 (grain 3)	5	12.3	2.4	0.00061	0.00012	2.57	85.3	9.7	LR
BU10_48 (grain 4)	2	11.7	2.2	0.00058	0.00012	2.52	92.4	24.5	LR
BU10_55 (grain 1)	1[a]	16.1	0.8	0.00079	0.00004			8.7	ER
BU10_55 (grain 1)	2[a]	21.7	1.2	0.00108	0.00005			7.9	LP
BU10_55 (grain 1)	3[a]	20.2	1.1	0.00100	0.00005			8.1	LP
BU10_55 (grain 1)	4[a]	14.8	1.1	0.00073	0.00005			11.9	LR
BU10_55 (grain 1)	5[a]	16.1	0.8	0.00079	0.00004			9.8	ER
BU10_55 (grain 1)	1	14.8	3.0	0.00073	0.00007	2.15	93.2	15.8	LR
BU10_61 (grain 2)	2	18.7	3.6	0.00093	0.00018	2.47	57.5	22.8	LP
BU10_61 (grain 1)	2	13.8	1.4	0.00068	0.00008	2.56	78.0	13.0	LR
BU10_61 (grain 1)	1	12.8	1.4	0.00063	0.00006	2.47	78.7	13.7	LR
BU10_61 (grain 2)	1	11.5	2.0	0.00057	0.00010	2.55	50.5	10.4	LR
BU10_74 (grain 1)	1	20.3	1.4	0.00100	0.00008	2.79	73.9	12.8	LP
BU10_74 (grain 2)	1	16.9	1.4	0.00084	0.00006	2.53	73.4	11.6	U
BU10_76 (grain 1)	1	10.8	0.8	0.00053	0.00004	2.50	88.7	7.9	LR
BU10_76 (grain 2)	2	10.7	1.0	0.00053	0.00004	2.26	87.1	10.5	LR
BU10_81 (grain 1)	1	15.0	2.0	0.00074	0.00010	2.51	84.7	12.4	LR
BU10_81 (grain 2)	3	15.0	2.0	0.00074	0.00010	2.59	86.5	11.6	LR
BU10_81 (grain 1)	2	14.5	2.0	0.00072	0.00010	2.45	80.8	12.6	LR
Early prograde age in the Jaishidanda Fm.;									
BU10_79 (grain 1)	1	15.0	2.4	0.00074	0.00012	2.43	63.5	13.6	EP

Remarks;

1 ^{204}Pb intensities corrected for $^{144}NdThO_2^{++}$ interference by using measured $^{143}NdThO_2^{++}$ intensities (average 0.161 cps), and $^{144}Nd/^{143}Nd$ isotopic abundance ratio = 1.95.

2 Common Pb correction using anthropogenic Pb compositions typical for southern California ($^{208}Pb/^{204}Pb = 38.34$); value from Sanudo-Wilhelmy and Flegal (1994), Geochim Cosmochim Acta, vol. 58, pp. 3315–3320.

3 Pb–Th relative sensitivity calibration using 554 monazite standard with $^{208}Pb/^{232}Th$ age = 45 Ma; Harrison et al. (1999), Journal of Petrology, vol. 40, pp. 3–19.

4 Pb–Th relative sensitivity calibration for three to ten bracketing standard analyses on the same mounts as the unknowns using a linear regression with a fixed slope (0.122) in measured ThO_2/Th vs. Pb–Th relative sensitivity for 554 standard.

5 Th/U ratios are based on uncorrected secondary ion intensities (primary beam intensity 2 nA ($^{16}O^-$), lateral spot dimensions ~10 μm, depth of analysis crater ~0.5 μm). For additional instrumental parameters, see Harrison et al. (1995), Earth Planet. Sci. Lett., vol. 133 (3–4), 271–282.

[a] LA-ICP-MS ages, EP: early prograde; LP: late prograde; ER: early retrograde; LR: late retrograde; U: uncertain.

GH samples from eastern Bhutan (Daniel et al., 2003). For rock compositions without allanite or xenotime, such as those in this study, monazite Y content links directly to prograde and retrograde reactions involving garnet (Kohn et al., 2004, 2005; Pyle and Spear, 1999, 2003; Pyle et al., 2001). Monazite that grows before prograde garnet or during garnet breakdown is characterized by high Y content, whereas monazite that grows in the presence of stable garnet tends to have low Y content. This occurs because, much like Mn, Y is sequestered in growing garnet, reducing Y contents of later-grown minerals (Foster et al., 2002; Kohn et al., 2005; Pyle and Spear, 1999, 2003; Pyle et al., 2001; Spear and Pyle, 2002). When partial melting occurs, monazite dissolves into the melt, while garnet continues to grow. Upon retrograde cooling and melt recrystallization, monazite grows either as new grains or as overgrowths on old (low-Y, low-Th) monazite cores while garnet dissolves. Y content in the monazite overgrowth should be high because the dissolution of garnet releases Y into the melt that is subsequently sequestered in monazite overgrowths (Kohn et al., 2005; Pyle and Spear, 2003).

In light of this well-understood chemical behavior, we selected GH samples that exhibited leucocratic segregations of quartz and feldspar in the expectation that these represented partial melts (Fig. 2; Daniel et al., 2003), and that monazite grains would have core–rim chemical systematics that could be related to partial melting reactions. Typical mineral assemblages are garnet + plagioclase + sillimanite + biotite + quartz + either muscovite or K-feldspar; several rocks contain kyanite or staurolite. In many rocks, garnets are rounded and replaced by sillimanite and biotite (Fig. 2), which we interpret as the retrograde melt crystallization reaction: garnet + K-feldspar + melt = biotite + sillimanite (reaction 12 of Spear et al., 1999, in a retrograde sense). In such rocks we would anticipate finding monazite with prograde low-Y cores mantled by retrograde high-Y rims (Kohn et al., 2004, 2005; Pyle and Spear, 2003), allowing a direct link between monazite chemistry and the heating vs. cooling of rocks.

4. Methods

4.1. Monazite mapping

All monazite grains were identified in polished thin-sections by reconnaissance mapping on the electron microprobe housed at the RUMrunner facility, Rutgers University, New Jersey. Garnet was present in all samples, but inclusions of monazite in garnet were uncommon and too small for analysis. For each monazite grain located, a backscattered (BSE) image was collected at low magnification to determine its textural relationship. Monazite grains (~20–100 μm) were either at the grain boundaries or inside of mica and feldspar crystals (Fig. 4A–F, Suppl. Figs. S1 and S2). Two to five grains from each sample were then mapped for elemental distribution (Y, Th, U, P, Ce, and Si) by electron microprobe using an accelerating voltage of 15 kV, a cup current of 200 nA, and a time per pixel of 30 ms. Considering the smaller size of grains and edge effects, beam mapping was preferred over stage mapping (which was performed only on two grains that were between ~100 and 200 μm). We used Y and Th mapping to guide the selection of spots for Th–Pb analyses because their zoning pattern correlates with different generations of metamorphic growth in a single monazite grain (e.g. Foster et al., 2002; Gibson et al., 2004; Kohn and Malloy, 2004; Kohn et al., 2005; Spear and Pyle, 2002) (see Section 3 above).

4.2. Monazite Th–Pb geochronology

Monazite grains mapped for Y, Th, U, Ce, and P were relocated in thin section then drilled out using a micro-diamond drill corer (1/4 in. or 1/8 in.). Grains were mounted with UCLA 554 monazite standard in epoxy rounds, and analyzed for U–Th–Pb isotopes using secondary ion mass spectrometry (SIMS) at the Department of Earth and Space Sciences, University of California, Los Angeles. Analysis of monazite followed analytical protocols described in Harrison et al. (1995). One to five analyses per grain were possible depending on crystal size. We used a primary beam intensity of 2 nA ($^{16}O^-$), a lateral spot size of ~10 μm, and a total analysis time of 10 min, which equates to a crater depth of ~0.5 μm. ^{204}Pb intensities were corrected for $^{144}NdThO_2^{++}$ interference by using measured $^{143}NdThO_2^{++}$ intensities (average 0.161 cps), and a $^{144}Nd/^{143}Nd$ isotopic abundance ratio of 1.95. Common Pb corrections were based on Pb compositions typical for southern California ($^{208}Pb/^{204}Pb = 38.34$; Sanudo-Wilhelmy and Flegal, 1994). Th–Pb relative sensitivity calibration is based on a 554 monazite standard with $^{208}Pb/^{232}Th$ age of 45 Ma (Harrison et al., 1999). Three to ten bracketing standard analyses were collected on the same mounts as the unknowns using a linear regression with a fixed slope (0.122) in measured ThO_2/Th vs. Pb–Th relative sensitivity for 554 standard. Th/U ratios are based on uncorrected secondary ion intensities. Th–Pb ages are reported with 2σ uncertainties (Table 1).

Because of questions relating to core–rim ages, we further analyzed two grains for Y and U–Th–Pb isotopes using a New-Wave UP-213 laser interfaced with a Thermo XSeries2 Quadrupole ICP-MS at Boise State University. Laser conditions included a spot size of 8 μm, repetition rate of 5 Hz, and fluence of c. 12 J/cm^2. Isotopes analyzed and their count times in ms were ^{44}Ca (10), ^{89}Y (10), ^{202}Hg (80), $^{204}Hg + ^{204}Pb$ (80), ^{206}Pb (120), ^{207}Pb (100), ^{208}Pb (150), ^{232}Th (10) and ^{238}U (40). ^{204}Pb was too low and uncertain for robust common Pb corrections, whereas $^{207}Pb/^{235}U$ ages were highly uncertain (≥25%), and $^{206}Pb/^{238}U$ ages appeared biased from excess ^{206}Pb. Consequently we focus on $^{208}Pb/^{232}Th$ ages. All ages were standardized against 44069 monazite (Aleinikoff et al., 2006).

For comparison to the LH monazite and other regional ages, we identified the youngest prograde and oldest retrograde mean ages for GH rocks by iterating on population averages until all ages within a mean were consistent to within 95% confidence. This resulted in averaging 5 ages for the youngest prograde mean age (used for calculating thrust rates below), and 18 ages for the oldest retrograde mean age.

5. Results

5.1. Map pattern of the MCT

In west-central Bhutan, a tectonic window through the overlying GH section exposes the Paro Formation below a top-to-the-south thrust contact (Figs. 1 and 3). South of this tectonic window, the Paro Formation is exposed again, and is bounded on both sides by north-dipping thrusts (Fig. 3). The southern of these two thrusts is an out-of-sequence structure that places the Paro Formation over GH paragneiss (Tobgay et al., 2010). Between the two exposures of the Paro Formation the GH section has been folded into a synform (Fig. 3). The southernmost MCT trace is located just ~15 km north of the Main Frontal Thrust (MFT), the southernmost structure of the Himalayan system. At its southernmost trace, the E–W striking and N-dipping MCT has GH rocks in its hanging wall and the LH Jaishidanda Formation in its immediate footwall.

5.2. Monazite chemical zonation mapping

Most zoning observed in GH monazite grains conforms to expectations regarding prograde melting and retrograde melt crystallization reactions, including low Y cores, high Y rims, and inverse correlation between Th and Y. Monazite grains from the same sample do not necessarily possess similar zoning patterns. Variations include grains exhibiting patchy Y or Th zoning, or strong zoning in one element and not another. Different chemistries and zoning patterns have been observed in other Himalayan anatectic rocks (e.g. Corrie and

Kohn, 2011; Kohn et al., 2005), but typically the chemistries and ages are reconcilable. For example, homogeneously low-Y grains may co-exist with homogeneously high-Y grains and grains with low-Y cores and high-Y rims. This simply reflects heterogeneities of mineral growth: some prograde monazite grains serve as nuclei for retrograde rims (zoned grains), others do not (homogeneously low Y), whereas still others nucleate and grow afresh during cooling (homogeneously high Y). This fact is further demonstrated by age distributions.

5.3. Monazite Th–Pb geochronology

Monazite ages obtained from multiple spots within individual grains show a wide range of Th–Pb ages with low-Y cores (high Th) typically about 10 Ma older than high-Y rims (e.g. Figs. S1a and S2c). Single samples can contain monazite cores as old as 24 Ma, as well as rims and entire grains that are as young as 10 Ma (e.g. BU08-1, Fig. S1a; BU10-61, Fig. S2d). Low Y (high Th) cores typically yielded the oldest ages while high Y (low Th) rims had the youngest ages. Many samples illustrate this, such as BU10-55, which exhibits a high Y, 14–16 Ma rim mantling a low Y, 20–22 Ma core. The seemingly anomalous 16.0 Ma age in a low-Y "core" region reflects the different regions sampled by X-rays (surface ~1 μm) vs. the laser (5–10 μm). Our LA-ICP-MS analysis at this spot almost immediately ablated through a thin low-Y, high $^{208}Pb/^{232}Th$ shell into a uniformly high-Y domain, from which the age was derived. That is, the X-rays represent the edge of the core, whereas the age represents the underlying rim. The northernmost two samples (BU08-1, and BU08-124; Fig. 3) also show high Y, 10–13 Ma rims around low-Y 21–24 Ma cores (Fig. S1a and c). Unlike other samples, BU08-4 exhibits a low Y core with a high Y rim, but the core and rim ages of 13–15 Ma are the same as retrograde ages from both laterally-equivalent samples and samples further to the south (Figs. 3 and 4D). For example, sample BU08-130 has grains with ages of 14.0 ± 0.6, 15.4 ± 0.6 and 13.4 ± 0.6 Ma. We interpret the entire BU08-4 grain as post-anatectic. As a whole, monazite grains from the central part of western Bhutan (Fig. 3; Figs. S1 and S2) have high Y content and correspond to growth ages that range from 15.4 ± 0.6 to 9.5 ± 0.8 Ma. Monazite grains sampled from rocks close to the southernmost trace of the MCT (Figs. 3, S2d, e, f, g, and h) record prograde ages of 20.3 ± 1.4 Ma, 18.7 ± 3.4 Ma, and possibly as young as 16.9 ± 1.4 Ma and retrograde rims between 15.0 ± 2.0 Ma and 10.7 ± 1.0 Ma. Monazite in the Jaishidanda Formation sample (BU10-79; Fig. 4F), which is located immediately below the MCT, yielded an age of 15.0 ± 2.4 Ma, which is similar to the oldest retrograde age of 15.0 ± 2.0 Ma immediately above the MCT.

6. Interpretations: Age and rate of thrusting

An age probability diagram of monazite ages from western Bhutan (Fig. 5A) emphasizes the age of the last growth of prograde subsolidus monazite (youngest high Th and low Y core) and the age of final melt crystallization during cooling (high Y rims). A population of youngest prograde ages (5 analyses) obtained from low-Y cores (high-Th) together give a mean and 2σ uncertainty of 20.8 ± 1.1 Ma (Fig. 5B). A mean of oldest retrograde ages (18 analyses) suggests that in situ melt crystallization (high-Y monazite rims) commenced at 15.1 ± 0.4 Ma (Fig. 5C).

The young population of GH monazite ages, (15.0 ± 2.4 to 9.5 ± 0.8 Ma) are from monazite with high Y rims or high homogeneous Y. Our sampling criteria (garnet in the presence of partial melt) together with garnet-reaction textures (Fig. 2) observed in thin sections, confirm that the dissolution of garnet in GH rocks is the source of Y that is sequestered in monazite during melt crystallization (Pyle and Spear, 1999; Spear et al., 1999). Partial melt is ubiquitous in GH rocks in western Bhutan, and because the MCT emplaces hot GH rocks (at least 700–750 °C; Corrie and Kohn, 2011; Daniel et al., 2003; Davidson et al., 1997) on cold (ca. 400–450 °C) LH rocks, the initiation of thrusting along the MCT and emplacement of GH rocks would be predicted to trigger a thermal perturbation in rocks in the immediate footwall (Jaishidanda Formation), driving prograde monazite growth in the footwall while simultaneously terminating prograde monazite dissolution and driving retrograde growth in the immediate hanging wall. Under this definition, the prograde monazite grains in GH rocks are pre-kinematic (i.e. associated with structural burial), while retrograde monazite grains in GH rocks are syn-kinematic to post-kinematic with respect to south-

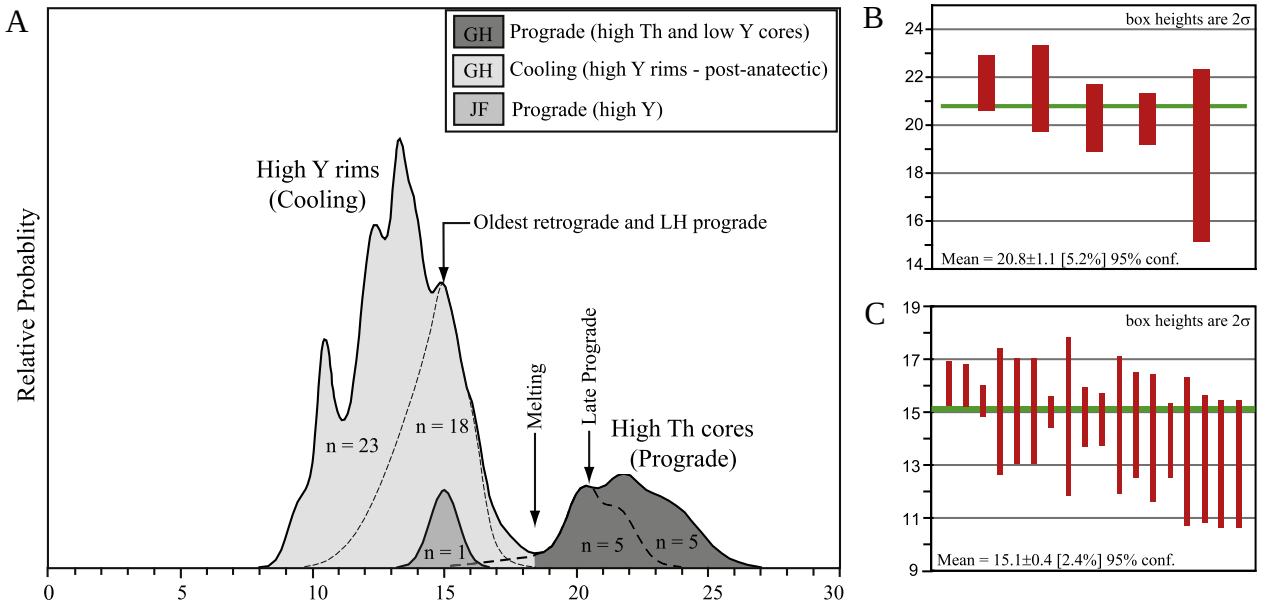

Fig. 5. A) Probability distribution plot of Greater Himalayan (GH) and Jaishidanda Formation (JF) monazite ages, with prograde and retrograde (cooling) divisions based on monazite chemistry. GH rocks contain compositionally-distinguishable prograde and retrograde monazite domains. B) A population of youngest prograde ages (5 analyses) obtained from low-Y cores (high-Th) giving a mean age of 20.8 ± 1.1 Ma (2σ uncertainty). C) A population of oldest retrograde or early crystallization ages obtained from high-Y rims (18 analyses) from GH rocks, giving a mean age of 15.1 ± 0.4 Ma (2σ uncertainty).

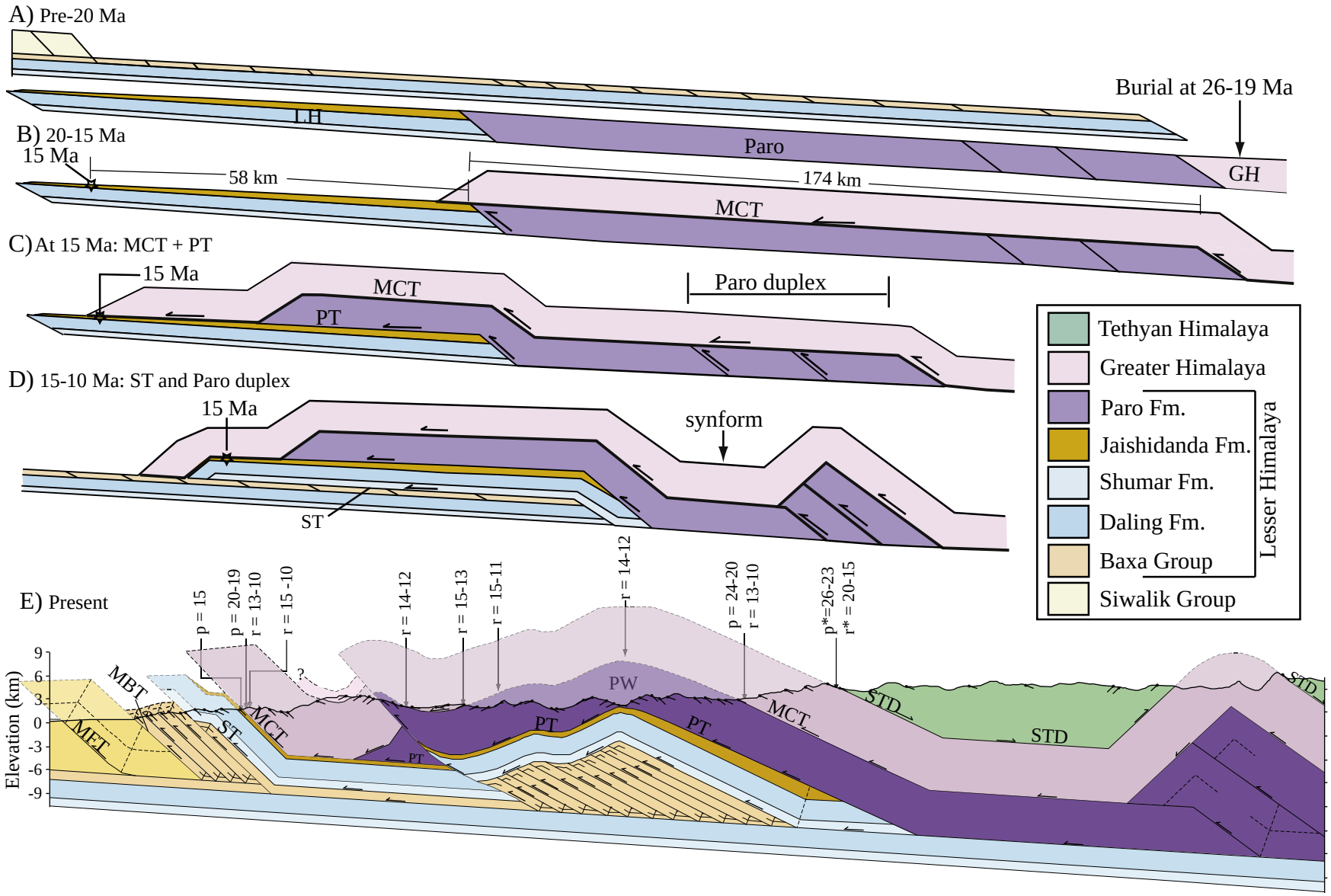

Fig. 6. Sequentially-restored cross-section illustrating the emplacement of GH rocks along the Main Central Thrust (MCT) in western Bhutan. A) Pre-20 Ma distribution of LH rocks and GH protoliths. B) Displacement along the MCT between 20 and 15 Ma that places GH rocks over a ~174 km-long Paro Formation section. C) Continuing motion on the MCT and displacement along the structurally-deeper Paro Thrust (PT) together bury a ~58 km-long Jaishidanda Formation section, resulting in prograde monazite growth in the Jaishidanda Formation at 15 Ma. D) Initiation of displacement along the Shumar Thrust (ST) and development of the Paro duplex in the hinterland between 15 and 10 Ma. E) Geologic cross-section (A–A′ in Fig. 3) across western Bhutan. Prograde (p) and retrograde (r) monazite ages are plotted across-strike. p* and r* denote prograde and retrograde ages, respectively, from Kellett et al. (2010).

directed thrusting. Therefore, the youngest prograde age of GH monazite grains limits the oldest possible initiation of south-directed thrust motion on the MCT. The age of prograde monazite growth in the Jaishidanda Formation (~15 Ma) constrains the time at which the MCT is emplaced over LH rocks at the southernmost extent of its trace. Thus the minimum duration of thrusting on the MCT in western Bhutan is from 20.8 ± 1.1 to 15.0 ± 2.4 Ma. Thrusting along the MCT is commonly interpreted to be coeval to north-vergent normal shearing along the South Tibetan detachment (STD) (e.g. Burchfiel et al., 1992; Chambers et al., 2011; Godin et al., 2006; Hodges et al., 1992). In the Lingshi syncline (LS; Figs. 1 and 3) in northwestern Bhutan, U–Pb ages of high Y monazite overgrowths in GH rocks in the immediate footwall of the outer-STD constrained the timing of displacement (shearing) to ca. 20–15 Ma (Kellett et al., 2010), which is equivalent to the minimum duration for MCT motion. The cessation of north-directed shearing on the outer-STD argues for termination of retrograde monazite growth at 15 Ma. However, young retrograde monazite grains between 15 and 9.5 Ma at the base of the GH section suggests that GH rocks were crystallizing and cooling until ~10 Ma, 5 Myr longer than motion on the outer-STD in the Lingshi syncline. Because cooling of the GH section is commonly thought to be driven by transport along the MCT, or underlying thrusts, it is possible that displacement on the MCT may have continued until ~10 Ma. This continued displacement must postdate motion on the outer-STD and may be linked to the development of a hinterland duplex that passively folded the northern MCT and the outer-STD, as discussed below (Fig. 6). This geometrical argument allows for limited transport along the MCT until ~10 Ma. Alternatively, growth of a duplex, directly under the Paro window would have focused erosion in this region, facilitating erosional cooling of the GH rocks while inhibiting continued thrusting along the MCT.

Sequential restoration of a balanced cross-section across western Bhutan allows estimation of displacement, which we relate to the timing of monazite growth. The two most important constraints in determining displacement magnitudes are the amount of overlap of GH rocks over LH rocks and the amount of overlap of the Paro Formation over more frontal LH rocks. The present-day north to south map extent of GH rocks is 140 km. Taking into account map-scale folding, the total overlap of GH rocks over LH rocks is 174 km (Figs. 3 and 6). The Paro Formation is underneath and parallel to GH rocks for a north–south distance of 50 km. Again taking into account map-scale folds, the minimum displacement on the Paro Thrust is 58 km. Thus, the collective amount of displacement on the MCT and Paro Thrust needed to bury the LH Jaishidanda Formation and grow monazite is 232 km (Fig. 6A–C). Determining the amount of shortening within LH rocks beneath the Paro Thrust and the geometry of the duplex which folds the Paro Thrust and MCT are subject to greater uncertainties. Shortening estimates from balanced cross sections are fundamentally controlled by the area between the mapped surface geology and the basal decollement, and the stratigraphic thickness of the rock units that are structurally repeated to fill this area. As a consequence, depending on the structural level of mapped exposure, shortening estimates for the same map data may vary. There are three possible scenarios for accommodating the area under the Paro Window, which include filling this space by repeating horses of the LH: 1) Baxa Group, 2) Daling–Shumar Group, or 3) Paro Formation. Because the Daling–Shumar Group and the Paro Formation are thicker than the Baxa Group, filling space beneath the Paro window with these formations decreases the total amount of shortening within this portion of the Himalayas. However, since the MCT and Paro Thrust must be emplaced over the total restored lengths of both the Paro Formation and the Daling–Shumar Group to bury the LH Jaishidanda sample, most of the shortening within the thrust belt in these 2 scenarios must predate 15 Ma. The first option, filling the space by repeating the Baxa Group, limits the amount of displacement on the MCT to the map constraints described previously. However, filling the space below the Paro window with thrusts that repeat the Paro Formation and the Daling–Shumar Group increases the distance the MCT must travel to reach the southernmost, lower LH rocks by 15 Ma. For the scenario that repeats the Daling–Shumar Group within the duplex, that distance is ~340 km, while the scenario that repeats the Paro Formation requires a distance of 325 km. Filling the space by repeating Baxa Group horses is preferred because: 1) it matches structural repetition of the Baxa Group observed in a similar tectonic window to the west in Sikkim (Fig. 1); and 2) it minimizes the rate of displacement on the MCT, keeping it at or below plate tectonic rates.

Combining a sequential reconstruction through western Bhutan (Fig. 6) with ages of monazite growth (Fig. 3) provides age estimates for thrust initiation, cessation and thrusting rates. From 26 to 21 Ma the GH section was buried, most likely by shortening and thickening in the overriding TH section (Aikman et al., 2008; Ding et al., 2005; Murphy and Yin, 2003; Patel et al., 1993; Robinson et al., 2001, 2006; Vannay and Hodges, 1996), promoting growth of prograde monazite. Displacement was initiated on the MCT sometime after 20.8 ± 1.1 Ma (Fig. 6B), resulting in the cessation of prograde monazite growth though the GH section and eventual burial of LH rocks at 15 Ma. Continued displacement along the frontal part of the MCT was accompanied by motion on the Paro Thrust (PT), which places the Paro Formation and the over-riding GH section over at least 232 km of LH rocks, in order to place the GH section over the Jaishidanda Formation sample (BU10-79) at 15 Ma (Fig. 6C). Based on this total displacement of ~230 km in 5.8 ± 2.6 Ma, we calculate an average rate of 40 mm/yr with lower and upper limits between 27 and 72 mm/yr. We suggest that between 15 and 10 Ma, the Shumar Thrust (ST) placed the Daling–Shumar Group (lower LH) over the Baxa Group (upper LH) in the foreland, and that continued motion occurred along the MCT as a duplex formed in the Paro Formation in the hinterland (Fig. 6D). This hinterland duplex passively folded overlying GH and TH rocks while sending an additional ~28 km of displacement towards the foreland on the MCT (Fig. 6D and E). This combined shortening of ~124 km along the Shumar Thrust (96 km) and Paro duplex (28 km) from 15 to 10 Ma provides a shortening rate of ~26 mm/yr. We propose that post-10 Ma shortening was accommodated by the formation of a duplex in the Baxa Group underneath the Paro Window and in front of the ST. The remaining shortening (165 km) from 10 to 0 Ma suggests continued slowing to rates of 16.5 mm/yr. The long-term average shortening rate from 20 Ma to present is ~28 mm/yr.

The rate of thrusting on the MCT in western Bhutan is higher than both the modern rates of convergence in the Himalaya, which is estimated at ~20 mm/yr from geodetic measurements across the Nepal Himalaya (Bettinelli et al., 2006; Bilham et al., 1997; Cattin and Avouac, 2000; Larson et al., 1999), and an MCT displacement rate of 22 ± 7 mm/yr, which is inferred from petrologic and thermal models in central Nepal (Kohn et al., 2004). With displacement rates possibly higher than 50 mm/yr, the MCT and Paro Thrust rates would be indistinguishable from the rate of relative convergence between the eastern edge of the Indian plate and the Asian plate at this time (van Hinsbergen et al., 2011). The rate we present for MCT displacement is strongly dependent on what loaded and buried the LH Jaishidanda Formation. Although it is possible that the thickened TH section that buried GH rocks to their peak P and T (Patel et al., 1993; Robinson et al., 2001; Vannay and Hodges, 1996), may have also contributed to the burial of the Paro and Jaishidanda formations to the south, we prefer to relate the prograde growth of monazite in LH (and GH) rocks to the timing of peak metamorphism. Mapped inverted temperature gradients in LH rocks in eastern Bhutan (Daniel et al., 2003; Long et al., 2011d) and the Paro Formation (Tobgay et al., 2010) strongly support the hypothesis that peak temperatures were reached via burial by a hot GH section carried by the MCT. In addition, if the Jaishidanda Formation section was initially buried by southward-displaced, cooler TH rocks, then we would expect prograde metamorphism to continue as the GH rocks were emplaced over the

Jaishidanda Formation. The lone prograde monazite age at 15 Ma suggests that the prograde burial path did not continue significantly past this time. Increasing the duration of heating of the Jaishidanda Formation would lower displacement rates for the MCT while maintaining the long-term shortening rate.

7. Discussion

A suite of data from this study and from previous studies in the Bhutan Himalaya allows us to evaluate variations in the duration and rate of thrusting along the MCT. In eastern Bhutan, prograde GH monazite grew from 26 to ~23 Ma (Chambers et al., 2011). Monazite from the immediate hanging wall of the MCT has a U–Pb age of 22 ± 1 Ma (not linked to monazite chemistry) that is interpreted to represent the initiation of displacement on the MCT (Daniel et al., 2003). In the MCT footwall, U–Pb ages of monazite between 20 and 18 Ma suggest a prograde age as a result of burial due to emplacement of the MCT over LH rocks (Daniel et al., 2003). This combination of monazite ages in the immediate hanging wall and footwall imply that MCT displacement in eastern Bhutan occurred between 23 and 20 Ma, with continued motion (until ~18 Ma) possibly linked to duplex formation in LH rocks (Long et al., 2011b). U–Pb ages of monazite from deformed leucogranite and migmatite higher in the GH section in eastern Bhutan suggest continued internal deformation and shearing within the GH section between 18 and 16 Ma as other parts of the system moved (Daniel et al., 2003). In the Sakteng klippe (SK; Fig. 1) in eastern Bhutan, initiation of north-directed normal shearing across the outer-STD would have cooled GH rocks in the immediate footwall and terminated prograde monazite growth. As a result, prograde GH monazites (26 to ~23 Ma) are pre-kinematic with respect to the north-directed shear across the STD and prograde monazite from the TH Chekha Formation (~23–21.5 Ma) are syn-kinematic with respect to shear across the STD (Chambers et al., 2011). This timing is consistent with the 3 Myr duration of MCT slip in eastern Bhutan from 23 to 20 Ma. Using 80–120 km of MCT displacement measured from balanced cross sections across eastern Bhutan (Long et al., 2011b), and a 3 Myr duration of displacement, we calculate an average motion rate of 3.3 ± 0.7 cm/yr, with lower and upper limits of 2.6 and 4 cm/yr.

The preceding compilation of monazite ages from eastern Bhutan highlights an east–west younging trend in initiation and duration of MCT displacement from 23–20 Ma in eastern Bhutan to ~20–15 Ma in western Bhutan. Although the MCT in western Bhutan post-dated displacement in eastern Bhutan by at least 3 Myr, the rate of displacement in western Bhutan (3–7 cm/yr) has substantial overlap with rates from eastern Bhutan (2.6–4 cm/yr). Our displacement rates of 3–7 cm/yr on the MCT are notably higher than the long-term average shortening rate (2.2 ± 0.5 cm/yr) within Bhutan. In addition, MCT displacement rates in Bhutan are higher than the ca. 2 cm/yr rate calculated for central Nepal based on geochronologic and thermobarometric data tied to thermal–mechanical models (e.g., Corrie and Kohn, 2011; Kohn, 2008; Kohn et al., 2004). A critical caveat is that model results are strongly dependent on the boundary conditions, thermal properties and convergence rates used (e.g. Corrie and Kohn, 2011). Generally, rates of displacement are held constant in models based on the similarities between geodetic convergence rates (19 ± 2.5 mm/yr; Bettinelli et al., 2006), Holocene shortening rates (21.5 ± 2 mm/yr; Lavé and Avouac, 2000) and rates of total shortening across the Himalaya from 25 Ma to present (18–22 mm/yr; e.g. DeCelles et al., 2001; Long et al., 2011b), thus precluding documenting potentially significant changes in rates though time. By applying a similar approach to the Kathmandu/Langtang region as we apply here, map patterns of the MCT and Ramgarh Thrust (RT) require minimum displacement amounts of 174 km and 168 km respectively (Pearson and DeCelles, 2005). Linking this displacement to Th–Pb in situ monazite ages from the same region (Kohn et al., 2004) suggests displacement rates of 2.5–4.3 cm/yr for the MCT (between 16 ± 1 and 10.5 ± 0.5 Ma) and rates that range from 3.4 to as high as 8.4 cm/yr (from 10.5 ± 0.5 to 8.9 Ma (muscovite cooling age) or 5 Ma (prograde LH duplex monazite)) for the RT. However, it is unlikely that shortening rates ever exceeded India–Asia convergence rates of 5 ± 0.5 cm/yr (Copley et al., 2010; van Hinsbergen et al., 2011). Combining these data from Bhutan and Nepal confirms that the MCT, which extends throughout the length of Himalayan orogen, may not have one unique age and rate of displacement. In addition, although long-term shortening rates are remarkably similar to those measured through GPS, we suggest these long-term shortening rates may be averaging periods of fast and slow shortening and potentially obscuring tectonically significant changes in rate.

8. Conclusions

The unique across-strike exposures in western Bhutan combined with chemically-defined Th–Pb in situ monazite ages from GH rocks immediately above the MCT in western Bhutan, allow us to constrain the age of displacement on the MCT, and with the aid of sequential cross-section reconstruction, estimate the rate of this displacement. The following conclusions can be drawn from our study:

1. The age of displacement on the MCT in western Bhutan is between 20 and 15 Ma, as defined by the youngest prograde GH monazite in the hanging wall and a prograde age of LH monazite in the footwall. This is also the same age duration as displacement and shearing along the outer-STD.
2. The calculated rate of displacement on the MCT in western Bhutan is between 3 and 7 cm/yr, which is similar to estimated plate tectonic rates over this window of time.
3. The age of displacement on the MCT varies across the Bhutan Himalaya. There is a ~3 Myr delay between the initiation of MCT displacement in eastern Bhutan and the initiation of MCT displacement in western Bhutan.
4. Variations in age, rate, and duration of MCT displacement may be the rule rather than the exception. Documenting how these rates vary in space and time will provide critical insight into the processes that govern the accommodation of plate convergence.

Supplementary materials related to this article can be found online at doi:10.1016/j.epsl.2011.12.005.

Acknowledgments

We would like to thank Dorji Wangda (the former Director General) of the Bhutan Department of Geology and Mines and Ugyen Wangda (Chief Geologist/Head) of the Geological Survey of Bhutan for their continued support. Also, we thank J. Delany, A. Schmitt, and P. Olin for their help with the electron probe, ion microprobe, and LA-ICP-MS. This work was supported by the National Science Foundation Grant Nos. EAR 0738522 to NM, EAR 0809428 and EAR 1048124 to MJK, and the Geological Society of America Graduate Student Research Grant to TT.

References

Aikman, A.B., Harrison, T.M., Ding, L., 2008. Evidence for early (>44 Ma) Himalayan crustal thickening. Tethyan Himalaya, southeastern Tibet. Earth Planet. Sci. Lett. 274, 14–23.

Aleinikoff, J.N., Schenck, W.S., Plank, M.O., Srogi, L., Fanning, C.M., Kamo, S.L., Bosbyshell, H., 2006. Deciphering igneous and metamorphic events in high-grade rocks of the Wilmington Complex, Delaware: morphology, cathodoluminescence and backscattered electron zoning, and SHRIMP U-Pb geochronology of zircon and monazite. Geol. Soc. Am. Bull. 118, 39–64.

Bettinelli, P., Avouac, J.-P., Flouzat, M., Jouanne, F., Bollinger, L., Willis, P., Chitrakar, G.R., 2006. Plate motion of India and interseismic strain in the Nepal Himalaya from GPS and DORIS measurements. J. Geod. 80, 567–589.

Bhattacharyya, K., Mitra, G., 2009. A new kinematic evolutionary model for the growth of a duplex — an example from the Rangit duplex, Sikkim Himalaya, India. Gondwana Res. 16, 697–715.

Bilham, R., Larson, K., Freymueller, J., 1997. Indo–Asian convergence rates in the Nepal Himalaya. Nature 311, 621–626.
Burchfiel, B.C., Chen, Z., Hodges, K.V., Liu, Y., Royden, L.H., Deng, C., Xu, J., 1992. The South Tibetan detachment system, Himalaya orogen: extension contemporaneous with and parallel to shortening in a collisional mountain belt. Geol. Soc. Am. Spec. Pap. 269, 41.
Catlos, E.J., Harrison, T.M., Kohn, M.J., Grove, M., Ryerson, F.J., Manning, C.E., Upreti, B.N., 2001. Geochronologic and thermobarometric constraints on the evolution of the Main Central Thrust, central Nepal Himalaya. J. Geophys. Res. 106, 16177–16204.
Catlos, E.J., Gilley, L.D., Harrison, T.M., 2002. Interpretation of monazite ages obtained via in situ analysis. Chem. Geol. 188, 193–215.
Catlos, E.J., Dubey, C.S., Harrison, T.M., Edwards, M.A., 2004. Late Miocene movement within the Himalayan Main Central Thrust shear zone, Sikkim, north-east India. J. Metamorphic Geol. 22, 207–226.
Cattin, R., Avouac, J.P., 2000. Modeling mountain building and the seismic cycle in the Himalaya of Nepal. J. Geophys. Res. 105 (B6), 13389–13407. doi:10.1029/2000JB900032.
Chambers, J., Parrish, R., Argles, T., Harris, N., Horstwood, M., 2011. A short duration pulse of ductile normal shear on the outer South Tibetan detachment in Bhutan: alternating channel flow and critical taper mechanics of the eastern Himalaya. Tectonics 30, 1–12.
Cherniak, D.J., Watson, E.B., Grove, M., Harrison, T.M., 2004. Pb diffusion in monazite: a combined RBS/SIMS study. Geochim. Cosmochim. Acta 68, 829–840.
Copley, A., Avouac, J.-P., Roye, J.-Y., 2010. India–Asia collision and the Cenozoic slowdown of the Indian plate: implications for the forces driving plate motions. J. Geophys. Res. 115, B03410. doi:10.1029/2009JB006634.
Corrie, S.L., Kohn, M.J., 2008. Trace-element distributions in silicates during prograde metamorphic reactions: implications for monazite formation. J. Metamorph. Geol. 26, 451–464.
Corrie, S.L., Kohn, M.J., 2011. Metamorphic history of the central Himalaya, Annapurna region, Nepal, and implications for tectonic models. Geol. Soc. Am. Bull.. doi:10.1130/B30376.1
Daniel, C.G., Hollister, L.S., Parrish, R.R., Grujic, D., 2003. Exhumation of the Main Central Thrust from lower crustal depths, eastern Bhutan Himalaya. J. Metamorph. Geol. 21, 317–334.
Davidson, C., Grujic, D., Hollister, L.S., Schmid, S.M., 1997. Metamorphic reactions related to decompression and synkinematic intrusion of leucogranite, High Himalayan Crystallines, Bhutan. J. Metamorph. Geol. 15, 593–612.
DeCelles, P.G., Robinson, D.M., Quade, J., Ojha, T.P., Garzione, C.N., Copeland, P., Upreti, B.N., 2001. Stratigraphy, structure, and tectonic evolution of the Himalayan fold–thrust belt in western Nepal. Tectonics 20, 487–509.
DeCelles, P.G., Gehrels, G.E., Najman, Y., Martin, A.J., Carter, A., Garzanti, E., 2004. Detrital geochronology and geochemistry of Cretaceous–Early Miocene strata of Nepal: implications for timing and diachroneity of initial Himalayan orogenesis. Earth Planet. Sci. Lett. 227, 313–330.
Ding, L., Kapp, P., Wan, X., 2005. Paleocene–Eocene record of ophiolite obduction and initial India–Asia collision, south central Tibet. Tectonics 24, TC3001. doi:10.1029/2004TC001729.
Foster, G., Gibson, H.D., Parrish, R., Horstwood, M., Fraser, J., Tindle, A., 2002. Textural, chemical and isotopic insights into the nature and behaviour of metamorphic monazite. Chem. Geol. 191, 183–207.
Gansser, A., 1964. Geology of the Himalaya. Wiley, Basel, pp. 1–289.
Gansser, A., 1983. Geology of the Bhutan Himalaya. Birkhauser Verlag Basel, Switzerland, p. 181.
Garzanti, E., 1999. Stratigraphy and sedimentary history of the Nepal Tethys Himalaya passive margin. J. Asian Earth Sci. 17, 805–827.
Gibson, H.D., Carr, S.D., Brown, R.L., Hamilton, M.A., 2004. Correlations between chemical and age domains in monazite, and metamorphic reactions involving major pelitic phases: an integration of ID-TIMS and SHRIMP geochronology with Y–Th–U X-ray mapping. Chem. Geol. 211, 237–260.
Godin, L., Grujic, D., Law, R., Searle, M.P., 2006. Crustal flow, extrusion, and exhumation in continental collision zones: an introduction. In: Law, R., Searle, M.P., Godin, L. (Eds.), Channel Flow, Ductile Extrusion, and Exhumation in Continental Collision Zones: Geological Society, London, Special Publication, 268, pp. 1–23. doi:10.1144/GSL.SP.2006.268.01.01.
Grujic, D., Hollister, L.S., Parrish, R.R., 2002. Himalayan metamorphic sequence as an orogenic channel: insight from Bhutan. Earth Planet. Sci. Lett. 198, 177–191.
Harrison, T.M., McKeegan, K.D., LeFort, P., 1995. Detection of inherited monazite in the Manaslu leucogranite by $^{208}Pb/^{232}Th$ ion microprobe dating: crystallization age and tectonic implications. Earth Planet. Sci. Lett. 133, 171–282.
Harrison, T.M., Grove, M., Lovera, O.M., Catlos, E.J., 1998. A model for the origin of Himalayan anatexis and inverted metamorphism. J. Geophy. Res. 103 (B11), 27,017–27,032.
Harrison, T.M., Grove, M., McKeegan, K.D., Coath, C.D., Lovera, O.M., Le Fort, P., 1999. Origin and episodic emplacement of the Manaslu intrusive complex, Central Himalaya. J. Petrol. 40, 3–19.
Harrison, T.M., Catlos, E.J., Montel, J.M., 2002. U–Th–Pb dating of phosphate minerals. Phosphates: Geochemical, Geobiological and Materials Importance. : Reviews in Mineralogy and Geochemistry, 48. Mineralogical Society of America, Washington, D.C., pp. 523–558.
Hodges, K.V., 2000. Tectonics of the Himalayas and southern Tibet from two perspectives. Geol. Soc. Am. Bull. 112, 324–350.
Hodges, K.V., Parrish, R.R., Housh, T.B., 1992. Simultaneous Miocene extension and shortening in the Himalayan orogen. Science 258, 1466–1469.
Hodges, K.V., Parrish, R.R., Searle, M.P., 1996. Tectonic evolution of the central Annapurna Range, Nepalese Himalayas. Tectonics 15, 1264–1291.
Kellett, D.A., Grujic, D., Warren, C., Cottle, J., Jamieson, R., Tenzin, T., 2010. Metamorphic history of a syn-convergent orogen-parallel detachment: the South Tibetan Detachment system, Bhutan Himalaya. J. Metamorphic Geology 28, 785–808.
Kohn, M.J., 2008. P–T–t data from central Nepal support critical taper and repudiate large-scale channel flow of the Greater Himalayan sequence. Geol. Soc. Am. Bull. 120, 259–273. doi:10.1130/B26252.1.
Kohn, M.J., Malloy, A.M., 2004. Formation of monazite via prograde metamorphic reactions among common silicates: implications for age determinations. Geochim. Cosmochim. Acta 68, 101–113.
Kohn, M.J., Wieland, M.S., Parkinson, C.D., Upreti, B.N., 2004. Miocene faulting at plate tectonic velocity in the central Himalaya, Nepal. Earth Planet. Sci. Lett. 228, 299–310.
Kohn, M.J., Wieland, M.S., Parkinson, C.D., Upreti, B.N., 2005. Five generations of monazite in Langtang gneisses: implications for chronology of the Himalayan metamorphic core. J. Metamorph. Geol. 23, 399–406.
Larson, K.M., Burgmann, R., Bilham, R., Freymueller, 1999. Kinematics of the India–Eurasia collision zone from GPS measurements. J. Geophys. Res. 104, 1077–1093.
Lavé, J., Avouac, J.P., 2000. Active folding of fluvial terraces across the Siwaliks Hills, Himalayas of central Nepal. J. Geophys. Res. 105 (B3), 5735–5770.
Le Fort, P., 1975. Himalayas: the collided range. Present knowledge of the continental arc. Am. J. Sci. 275-A, 1–44.
Long, S., McQuarrie, N., 2010. Placing limits on channel flow: insights from the Bhutan Himalaya. Earth Planet. Sci. Lett. 290, 375–390.
Long, S.P., McQuarrie, N., Tobgay, T., Rose, C.V., Gehrels, G., Grujic, D., 2011a. Tectonostratigraphy of the Lesser Himalaya of Bhutan: implications for the stratigraphic architecture of the Northern Indian Margin. Geol. Soc. Am. Bull. 123, 1406–1426. doi:10.1130/B30202.1.
Long, S., McQuarrie, N., Tobgay, T., Grujic, D., 2011b. Geometry and crustal shortening of the Himalayan fold–thrust belt, eastern and central Bhutan. Geol. Soc. Am. Bull.. doi:10.1130/B30203.1
Long, S.P., McQuarrie, N., Tobgay, T., Hawthorn, J., 2011c. Quantifying internal strain and deformation temperature in the Eastern Himalaya, Bhutan: implications for the evolution of strain in thrust sheets. J. Struct. Geol. 33, 579–608. doi:10.1016/j.jsg.2010.12.011.
Long, S., McQuarrie, N., Tobgay, T., Grujic, D., Hollister, L., 2011d. Geologic map of Bhutan. The Journal of Maps, v2011, pp. 184–192, 1:500,000-scale, doi:10.4113/jom.2011.1159.
McQuarrie, N., Robinson, D., Long, S., Tobgay, T., Grujic, D., Gehrels, G., Ducea, M., 2008. Preliminary stratigraphic and structural architecture of Bhutan: implications for the along-strike architecture of the Himalayan orogen. Earth Planet. Sci. Lett. 272, 105–117.
Murphy, M.A., Yin, A., 2003. Structural evolution and sequence of thrusting in the Tethyan fold–thrust belt and Indus–Yalu suture zone, southwest Tibet. Geol. Soc. Am. Bull. 115 (1), 21–34.
Parrish, R.R., 1990. U–Pb dating of monazite and its application to geological problems. Can. J. Earth Sci. 27, 1431–1450.
Patel, R.C., Sandeep, S., Asokan, A., Manickavasagam, R.M., Jain, A.K., 1993. Extensional tectonics in the Himalayan orogen Zanskar, NW India. In: Trelaor, P.J., Searle, M.P. (Eds.), Himalayan Tectonics, Geological Society Special Publication, 74, pp. 445–459.
Pearson, O.N., DeCelles, P.G., 2005. Structural geology and regional tectonic significance of the Ramgarh thrust, Himalayan fold–thrust belt of Nepal. Tectonics 24, TC4008. doi:10.1029/2003TC001617.
Pyle, J.M., Spear, F.S., 1999. Yttrium zoning in garnet: coupling of major and accessory phases during metamorphic reactions. Geol. Mater. Res. 1, 1–49.
Pyle, J.M., Spear, F.S., 2003. Four generations of accessory-phase growth in low-pressure migmatites from SW New Hampshire. Am. Mineral. 88, 338–351.
Pyle, J.M., Spear, F.S., Rudnick, R.L., McDonough, W.F., 2001. Monazite–xenotime–garnet equilibrium in metapelites and a new monazite–garnet thermometer. J. Petrol. 42, 2083–2107.
Robinson, D.M., DeCelles, P.G., Patchett, P.J., Garzione, C.N., 2001. The kinematic evolution of the Nepalese Himalaya interpreted from Nd isotopes. Earth Planet. Sci. Lett. 192, 507–521.
Robinson, D.M., DeCelles, P.G., Copeland, P., 2006. Tectonic evolution of the Himalayan thrust belt in western Nepal: implications for channel flow models. Geol. Soc. Am. Bull. 118, 865–885.
Sanudo-Wilhelmy, S.A., Flegal, A.R., 1994. Temporal variations in lead concentrations and isotopic composition in the Southern California Bight. Geochim. Cosmochim. Acta 58, 3315–3320.
Smith, H.A., Giletti, B.J., 1997. Lead diffusion in monazite. Geochim. Cosmochim. Acta 61, 1047–1055.
Spear, F.S., 2010. Monazite–allanite phase relations in metapelites. Chem. Geol. 279, 55–62.
Spear, F.S., Pyle, J.M., 2002. Apatite, monazite and xenotime in metamorphic rocks. Rev. Mineral. 48, 293–335.
Spear, F.S., Kohn, M.J., Cheney, J.T., 1999. P–T paths from anatectic pelites. Contrib. Mineral. Petrol. 134, 17–32.
Tobgay, T., Long, S., McQuarrie, N., Ducea, M., Gehrels, G., 2010. Using isotopic and chronologic data to fingerprint strata: the challenges and benefits of variable sources to tectonic interpretations, the Paro Formation, Bhutan Himalaya. Tectonics 29, TC6023. doi:10.1029/2009TC002637.
Tukuoka, T., Takayasu, K., Yoshida, M., Hisatomi, K., 1986. The Churia (Siwalik) Group of the Arung Khola area, west central Nepal. Shimane, Japan: Memoirs of the Faculty of Science, Shimane University, Vol. 20, pp. 135–210.
van Hinsbergen, D.J.J., Steinberger, B., Doubrovine, P.V., Gassmoller, R., 2011. Acceleration and deceleration of India–Asia convergence since the Cretaceous: roles of mantle plumes and continental collision. J. Geophys. Res. 116, B06101. doi:10.1029/2010JB008051.

Vannay, J.-C., Hodges, K.V., 1996. Tectonomorphic evolution of the Himalayan metamorphic core between the Annapurna and Dhaulagiri, central Nepal. J. Metamorph. Geol. 14, 635–656. doi:10.1046/j.1525-1314.1996.00426.x.

Wing, B.N., Ferry, J.M., Harrison, T.M., 2003. Prograde destruction and formation of monazite and allanite during contact and regional metamorphism of pelites: petrology and geochronology. Contrib. Mineral. Petrol. 145, 228–250.

Yin, A., 2006. Cenozoic tectonic evolution of the Himalayan orogen as constrained by along-strike variation of structural geometry, exhumation history, and foreland sedimentation. Earth Sci. Rev. 76, 1–131. doi:10.1016/j.earscirev.2005.05.004.

Yin, A., Harrison, T.M., 2000. Geologic evolution of the Himalaya–Tibetan orogen. Annu. Rev. Earth Planet. Sci. Lett. 28, 211–280.

Yin, A., Dubey, C.S., Kelty, T.K., Webb, A.A.G., Harrison, T.M., Chou, C.Y., Celerier, J., 2010. Geologic correlation of the Himalayan orogen and Indian craton: Part 2: structural geology, geochronology, and tectonic evolution of the Eastern Himalaya. Geol. Soc. Am. Bull. 122, 360–395. doi:10.1130/B26461.1.